JACS
JOURNAL OF THE AMERICAN CHEMICAL SOCIETY

Communication

pubs.acs.org/JACS

Transmembrane Potential across Single Conical Nanopores and Resulting Memristive and Memcapacitive Ion Transport

Dengchao Wang, Maksim Kvetny, Juan Liu, Warren Brown, Yan Li, and Gangli Wang*

Department of Chemistry, Georgia State University, Atlanta, Georgia 30302, United States

Supporting Information

ABSTRACT: Memristive and memcapacitive behaviors are observed from ion transport through single conical nanopores in SiO_2 substrate. In $i-V$ measurements, current is found to depend on not just the applied bias potential but also previous conditions in the transport-limiting region inside the nanopore (history-dependent, or memory effect). At different scan rates, a constant cross-point potential separates normal and negative hysteresis loops at low and high conductivity states, respectively. Memory effects are attributed to the finite mobility of ions as they redistribute within the negatively charged nanopore under applied potentials. A quantative correlation between the cross-point potential and electrolyte concentration is established.

Memory effects refer to the response signal being determined by not only external stimuli but also the former states or the history of the system.[1] In electronics, resistive, capacitive, and inductive elements with memory effects differ from their traditional counterparts in that their magnitudes vary with respect to time rather than being constant. The resulting history-dependent properties are defined as memristive, memcapacitive, and meminductive behaviors, respectively.[2] Memory effects originate from the dynamic properties of charge carriers (electron or ions).

Ion transport (IT) confined at nanometer-scale pores and channels has received considerable recent interest.[3] Strongly affected by nanodevice geometry and charged interface, interesting diode-type nonlinear $i-V$ conductivity responses are frequently observed under steady-state (SS) measurements, known as ionic current rectification (ICR).[4] Both non-SS and SS IT affected by the structurally defined nanoconfinement unveil fundamental information for the further development of nanoelectronics and high-density electrochemical energy storage and conversion devices.[5] For example, this IT process directly reflects the charging/discharging of a supercapacitor with a nonparallel electrode surface (electrochemical capacitor) at the nanometer scale.

Artificial solid-state nanopores and nanochannels can be regarded as mimics of protein ion channels and have been developed for sensing applications.[6] The current signal, resulting from the movement of ions, is determined by the most resistive region, normally close to the smallest cross-sectional area in the pore channel. Based on the Coulter-counter concept, various nanopores and nanochannels are developed for stochastic sensing and DNA sequencing.[7] Dynamic responses of IT at non-SS are obviously more relevant to stochastic sensing applications, where the signal is based on the disturbance of ion flux by analytes at the signal-limiting nanopore region. Importantly, the distribution of ion flux is not uniform inside charged conical nanopores; it is determined by both external applied potential and intrinsic nanopore surface potential. Quantification of their respective impacts on ion flux would require information inaccessible by the most commonly used SS conductivity measurements.

Frequency domain impedance analysis of IT through conical nanopores reveals multiple processes with different time constants.[8] An apparent inductive response was detected in the low frequency range (sub-1 kHz) in the high conductivity state, while an additional capacitive feature is observed in the low conductivity state at a comparable frequency range. Molecular dynamics simulation suggested negative capacitance in IT through single nanopores with symmetric geometry.[2] The proposed negative capacitance mechanism is in excellent agreement with the apparent inductive responses observed in impedance measurements.

In this paper, time and frequency domain ionic current responses of single conical glass nanopores are analyzed. Under selected scan rates and potential ranges, interesting hysteresis loops corresponding to normal and negative capacitance in IT through single nanopores are discovered. Measurements directly reveal memory effects in IT near the charged interface at nanometer scale. Furthermore, the effective transmembrane potential across the nanodevice substrate is noninvasively determined under measurement conditions.

High and low conductivity states of a conical nanopore during the measurements are illustrated in Scheme 1. Nanopore preparation and electrochemical measurements follow previous reports;[9] see the Supporting Information (SI) for details. A conical glass nanopore is loaded with KCl solution (inside) and then immersed in the same KCl solution (outside). Two Ag/AgCl wires are used as inside and outside electrodes to control the applied potential waveform (V_a). The detected current signal is limited by the most resistive region along the circuit, originating from ion flux near the nanopore orifice. Meanwhile, fixed negative charges at the substrate−solution interface (due to deprotonation of silanol groups on glass surface) establish a surface potential profile. Φ_0 corresponds to the surface potential induced by surface excess charges following the classic double-layer (DL) description. In a conical nanopore (half-cone angle θ), the surface electrostatic field, perpendicular

Received: November 28, 2011
Published: February 7, 2012

dx.doi.org/10.1021/ja211142e | J. Am. Chem. Soc. 2012, 134, 3651−3654

Scheme 1. Visual Representation of Ion Transport through a Conical Nanopore (Half-Cone Angle θ)[a]

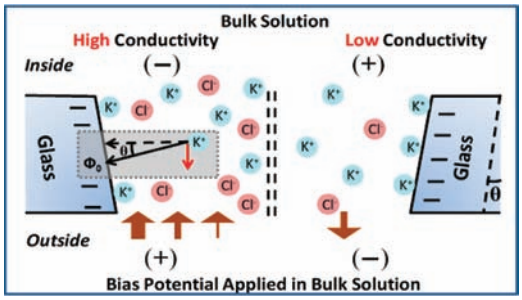

[a]Left and right sides show opposite applied potential polarities that establish high and low conductivity states, respectively. Block arrows at the bottom represent the corresponding K^+ flux driven by external bias potential. Impacts of surface potential on K^+ flux are illustrated in the dotted line-frame. Not drawn to scale.

to the surface, will have a component along the direction of ion current, shown as a red arrow in the gray dotted line frame of Scheme 1. This component (correlation factor of $\sin\theta$) will establish an effective potential profile across the membrane (V_m) superimposed with the applied potential V_a. The component of electrostatic field normal to V_a does not directly affect the measured current but changes the ion distribution within the nanopore.

The $i-V$ responses of a 45-nm-radius nanopore at different scan rates in 10 mM KCl are presented in Figure 1; data for 50, 100, and 1000 mM KCl are shown in Figure SI-1. The $i-V$ curves show obvious ICR, in agreement with literature.[10] For conical nanopores with negatively charged surfaces, the high conductivity state is established if positive bias potential is applied externally relative to the inside electrode. By increasing the scan rate, the current amplitude slightly increases at the low conductivity state but decreases more significantly at the high conductivity state. The overall reduction in the rectification factor as scan rate increases is qualitatively in agreement with previous experimental and computation studies by Zhang and Girault, respectively,[11] in which significant charging current was observed at much higher scan rates. The rectified ionic conductivity changes at different scan rates, indicating time-dependent resistance, in accordance with the memresistive effects described in electronics.

The current amplitudes of different scan directions (−1.0 to +1.0 V vs +1.0 to −1.0 V) are different and cross at a common potential near zero. The two hysteresis loops are separated by this constant cross-point potential (see Figure 1A). Analogous to the isosbestic point in spectroscopic measurements, this potential indicates the transition between the high and low conductivity states. As seen in the enlarged view in Figure 1A, the cross-point potential is independent of the scan rates employed. While the loop at the low conductivity state displays normal capacitive responses, the loop at the high conductivity state exhibits "negative" capacitance with respect to a normal capacitive feature. In other words, the current is higher if the applied potential is scanned from higher to lower conductive state (from +1.0 toward 0 V). The capacitive and ICR features are highly consistent for repeated scans and independent of the initial potential or scan directions. The cross-point potential is independent of the potential range if the potential window is beyond ~400 mV from the cross potential (Figure SI-2). The first scan is generally discarded in this analysis. For reference,

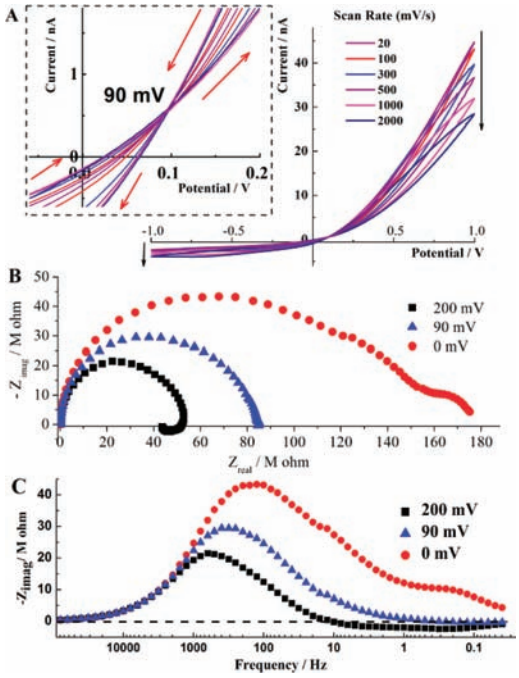

Figure 1. (A) Overlaid $i-V$ curves at different scan rates in 10 mM KCl. Cross-point potential remains at 90 mV at all scan rates. Black arrows next to the curves indicate changes in current with increase of scan rate. Red arrows in the inset illustrate direction of potential scan. Impedance spectra taken above, below, and at the cross-point potential are plotted in the form of Nyquist (B) and Bode (C) plots.

the scan rate dependence of a solid-state resistor−capacitor (RC) circuit is provided in Figure SI-3, where a normal capacitive loop is consistently observed.

Normal and "negative" capacitive behaviors in low and high conductivity states are confirmed by impedance analysis. In the Nyquist plot (Figure 1B), an additional RC loop was observed at the low conductivity state (0 mV), while an apparent inductive loop in the fourth quadrant was observed at the high conductivity state (200 mV). The additional low frequency loops, better seen in the Bode plot (Figure 1C), diminished if the DC bias potential was held at the cross-point (90 mV). A semicircle in the Nyquist plot or a single peak in the Bode plot indicates a simple one-time-constant mass transport process. With a slight deviation from this cross-point potential, the impedance responses transform from inductive to capacitive behavior, or vice visa. The cross-point potential separates the signature of IT through the nanopore and reflects the nature of the nanopore geometry and surface charge. This discussion is further validated by equivalent circuit fitting results (Figure SI-4).

A constant cross-point potential connecting two hysteresis loops at different scan rates in $i-V$ curves has been observed from other nanopores (>10) (see representative results in Figures SI-5 and SI-6). Furthermore, the cross-point potential is confirmed to be largely independent of asymmetry of the two Ag/AgCl electrodes. By switching the position of the inside and outside electrodes, a slight shift at ~5−10 mV was observed (Figure SI-7). The value is much less than the cross-point potential. Those highly reproducible results rule out the possibility of measurement artifacts such as electrode preparation or instrumental offset.

The nonzero cross-point potential is independent of scan rate but varies in different electrolyte concentrations. As shown

dx.doi.org/10.1021/ja211142e | J. Am. Chem. Soc. 2012, 134, 3651−3654

in Figure 2A, the cross-point potential, referred to as the effective transmembrane potential (V_M), decreases and

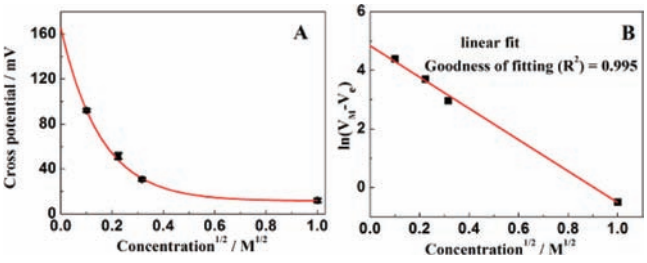

Figure 2. Correlation of electrolyte concentration with cross-point potential. At each concentration, cross-point potential was averaged from i−V curves with scan rates ranging from 100 to 2000 mV/s. The fitting was performed with $V = V_0 \exp(-C^{1/2}/A) + V_e$, or its natural logarithm as shown in (B).

approaches an asymptote with increasing electrolyte concentration. Quantitatively, the cross-point potential displays an exponential dependence on the square root of concentration, which is directly adapted from the Debye length description in classic DL theory:[12]

$$V = V_0 \exp(-C^{1/2}/A) + V_e \quad (1)$$

where C is electrolyte concentration, A a constant related to temperature, and V_0 an effective surface potential, and V_e addresses nonideal factors in the measurements. This correlation is further illustrated by the excellent linear fitting in Figure 2B. Analogous to the potential profile described in classic DL theory, at a certain electrolyte concentration C, eq 1 describes this screening effect quantitatively. As the electrolyte concentration increases, the electrostatic interactions between mobile ions and surface charges are more effectively screened. Correspondingly, the cross-point potential, or V_M, which reflects the effective surface potential along the transport direction, will decrease. Therefore, V_0 represents the surface potential that is a function of surface excess charges or surface charge density. Based on the plot, V_0 = 153 mV. Similar analysis of two other nanopores gives V_0 = 150 and 115 mV for 200- and 80-nm-radius nanopores, respectively (Figure SI-8). The amplitude of V_0 is qualitatively in agreement with the degree of ICR, in which the high conductivity states are known to depend on surface charge density.[13] If the electrostatic interaction becomes negligible at sufficiently high electrolyte concentration, the cross-point potential should approach zero. Experimentally, thermal fluctuations, solubility of the electrolyte, and asymmetry of the two Ag/AgCl electrodes limit the measurement resolution, expressed as $V_e \approx 5-10$ mV. Since the surface electric field at any position inside the nanopore is determined by electrolyte concentration, nanopore geometry, and surface excess charges (i.e., V_0), the cross-point potential is independent of measurement conditions such as scan rate.

Next we demonstrate the diverging capacitance and charge−potential (Q−V) dependence to correlate with the theoretical predictions of nanopore memcapacitance.[2] Memory effects can be quantitatively described by changes of charges at specific potentials. The instantaneous transported charge (Q) in Figure 3A is calculated from

$$Q = I\Delta t = I\Delta V/v \quad (2)$$

where v is the scan rate and I the measured current. The potential step (ΔV) was at 1 mV intervals. This is the instantaneous transported charge through the nanopore. Unlike the typical capacitor charging/discharging process, charge continues to accumulate at the high conductivity state, even though the bias potential decreases (process 4 in Figure 3A).

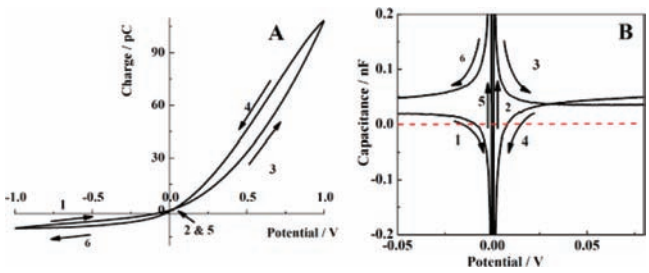

Figure 3. Memory effects of transported charges (A) and nanopore capacitance (B) at controlled potential. The data were collected in 100 mM KCl at a scan rate of 1 V/s. The arrows and numbers along the curve indicate the direction of potential scan.

The gap between the two curves (segment 4 vs 3 or 1 vs 6) directly reflects the memory effects. From Figure 3B, the history-dependent capacitance ($C = Q/V$) is evident with the dashed line highlighting zero and the crossing of curves 3 and 4; see Figure SI-9 for the corresponding responses of a solid-state RC. Quantification and analysis of the residual memory charges will be reported separately.

The mechanism of the observed memory effects is proposed in the context of finite mobility of ions. Four scenarios are qualitatively illustrated in Scheme 2. Separated by the cross-

Scheme 2. Visual Representation of the Mechanism Governing IT Memory Effects in Nanopores[a]

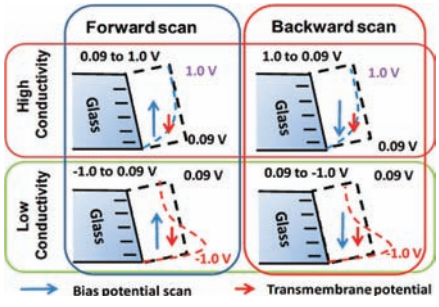

[a]Blue arrow represents direction of DL polarization resulting from the scan direction of the applied potential: forward scan is defined as a transition from lower to higher conductivity states; backward scan is the reverse. Red arrow illustrates direction of electric field resulting from negative charges on a glass substrate. Dashed lines illustrate undisturbed and polarized DL structure; they do not reflect conductivity profiles reported in simulation studies.

point potential (e.g., 0.090 V in 10 mM), the top two panels illustrate the high conductivity state while the bottom two represent the low conductivity state. At rest with no bias potential applied, the diffuse layer extends parallel from the surface. The black dashed line illustrates the DL structure (the Debye length plane). When a positive bias potential (+1.0 V) relative to the pore interior is applied (high conductivity state), the diffuse layer (ion distribution) is polarized toward the pore interior, shown as a blue dashed line. At low conductivity states (−1.0 V), the displacement is reversed toward the pore

dx.doi.org/10.1021/ja211142e | J. Am. Chem. Soc. 2012, 134, 3651−3654

exterior, shown as a red dashed line. Since the dashed lines illustrate the impacts of surface potential, the trend is actually opposite to the simulated overall conductivity profiles inside a nanopore.

Next we discuss the differences between forward and backward current. The dynamics of DL polarization (ion redistribution) within a nanopore is not instantaneous with respect to the change of applied potential; the detected current is affected by its former state, the conductivity at the previous applied potential. For forward scan (from lower to higher conductivity state) the current lags to the former state with lower conductivity; for backward scan the current "memorizes" the former higher conductivity state. If the time scale of this hysteretic process is comparable to that of measurement, forward current will be lower than backward current.

The effective transmembrane potential (V_M) is a function of the surface electric field component along the ion current direction (by $\sin\theta$) accumulative over the whole effective nanopore length. Established by negative surface excess charges, this component maintains its polarity/direction (red arrow in Scheme 2). The resulting surface potential profile is against the direction of diffuse layer polarization (or ion redistribution) driven by the applied potential in the forward scan, while in the backward scan the tendency of ion redistribution driven by the two potential profiles has the same direction. Accumulatively, an offset (cross-point) potential separates the high and low conductivity states as well as the negative and positive phase shifts in impedance measurements. With our quantitative fitting by Comsol simulation of measured $i-V$ responses of single nanopores of systematically varied ionic strengths,[13] quantitative correlation of the transmembrane potential with the surface charge density and half-cone angle of individual nanopores is underway.

The time scale of the polarization of ion distribution inside a nanopore can be estimated directly from the ion mobility and the applied potential. The ion mobility of K^+ and Cl^- at $\sim 8 \times 10^{-4}$ cm^2 s^{-1} V^{-1} is used. At 0.5 V applied potential, assuming the effective pore depth at 1×10^{-4} cm, the average velocity would be 4 cm/s. The time for ions in the middle of the nanopore to migrate out of the current-limiting region with negligible surface interaction would be 1.25 ms. This corresponds to the fast process shown in impedance measurements in Figure 1C (800 Hz). At 1 mV potential intervals in $i-V$ measurements (e.g., from 0.5 to 0.501 V or from 0.5 to 0.499 V), the scan rate to observe this memory effect due to noninstantaneous ion redistribution, or a difference in forward and backward currents, would be 1 mV/1.25 ms, or 0.8 V/s. This corresponds to the polarization of ion distribution at the whole current-limiting nanopore region, thus the maximum memcapacitive effects. The surface electric field would tend to maintain the ion distribution inside the nanopore and induce a range of scan rates for analyzing this interaction and the resulting memory effects. If the scan rate is too slow (20 times slower than 0.8 V/s, 0.020 V/s) the phase shift would be negligible and resistance/memresistance behavior will dominate the measurements. At very high scan rate (20 times faster than 0.8 V/s, 8 V/s) the capacitive behaviors corresponding to the charging/discharging of external interfaces of glass substrate will dominate the measurements. The earlier experimental and computation studies confirm the above discussion.[11] The ICR inversion at extremely low ionic strength in the simulation is very challenging to experimentally confirm at the single nanopore level due to low current signal.

In summary, memory effects have been discovered in ion transport confined by nanoscale geometry and interface. In time and frequency domain electrochemical measurements, a nonzero cross-point potential separates normal RC behaviors from apparent inductive (or capacitive with a negative phase shift) behaviors in the low frequency range (sub-1 kHz). The cross-point potential is quantitatively correlated to solution ionic strength, through which the effective surface potential inside single nanopores is noninvasively determined. The physical origin of the memory effects is attributed to the relative kinetics between the stimulus (applied potential) and the responding IT, which induces polarization of the diffuse layer within the current-limiting region in nanopores affected by ion mobility and surface potential. The analysis provides fundamental insight into the structure and dynamics of an electrical DL at the nanometer scale.

■ ASSOCIATED CONTENT

Ⓢ Supporting Information

Experimental details and analytical data. This material is available free of charge via the Internet at http://pubs.acs.org.

■ AUTHOR INFORMATION

Corresponding Author

glwang@gsu.edu

Notes

The authors declare no competing financial interest.

■ ACKNOWLEDGMENTS

J.L. is an MBD fellow at GSU. J.L. and G.W. acknowledge the summer support from the Fluid Interface Reactions, Structures and Transport (FIRST) EFRC funded by DOE under Award No. ERKCC61.

■ REFERENCES

(1) Pershin, Y. V.; Ventra, M. D. *Adv. Phys.* **2011**, *60*, 145.

(2) Krems, M.; Pershin, Y. V.; Ventra, M. D. *Nano Lett.* **2010**, *10*, 2674.

(3) (a) Siwy, Z. S.; Howorka, S. *Chem. Soc. Rev.* **2010**, *39*, 1115. (b) Daiguji, H. *Chem. Soc. Rev.* **2010**, *39*, 901. (c) Schoch, R. B.; Han, J.; Renaud, P. *Rev. Mod. Phys.* **2008**, *80*, 839.

(4) (a) Siwy, Z.; Gu, Y.; Spohr, H. A.; Baur, D.; Wolf-Reber, A.; Spohr, R.; Apel, P.; Korchev, Y. E. *Europhys. Lett.* **2002**, *60*, 349. (b) Stein, D.; Kruithof, M.; Dekker, C. *Phys. Rev. Lett.* **2004**, *93*, 035901.

(5) Itoi, H.; Nishihara, H.; Kogure, T.; Kyotani, T. *J. Am. Chem. Soc.* **2011**, *133*, 1165.

(6) Martin, C. R.; Siwy, Z. S. *Science* **2007**, *317*, 331.

(7) Schibel, A. E. P.; An, N.; Jin, Q.; Fleming, A. M.; Burrows, C. J.; White, H. S. *J. Am. Chem. Soc.* **2010**, *132*, 17992.

(8) Feng, J. Y.; Liu, J.; Wu, B. H.; Wang, G. L. *Anal. Chem.* **2010**, *82*, 4520.

(9) (a) Zhang, B.; Zhang, Y.; White, H. S. *Anal. Chem.* **2004**, *76*, 6229. (b) Wang, G.; Zhang, B.; Wayment, J. R.; Harris, J. M.; White, H. S. *J. Am. Chem. Soc.* **2006**, *128*, 7679.

(10) Siwy, Z. S. *Adv. Funct. Mater.* **2006**, *16*, 735.

(11) (a) Guerrette, J. P.; Zhang, B. *J. Am. Chem. Soc.* **2010**, *132*, 17088. (b) Momotenko, D.; Girault, H. H. *J. Am. Chem. Soc.* **2011**, *133*, 14496.

(12) Bard, A. J.; Faulkner, L. R. *Electrochemical methods: fundamentals and applications*, 2nd ed.; John Wiley & Sons: New York, 2001.

(13) Liu, L.; Maksim, K.; Feng, J. Y.; Wang, D. C.; Wu, B. H.; Warren, B.; Wang, G. L. *Langmuir* **2012**, *28*, 1588.